High-Resolution Bidirection Estimation Based on the SAGE Algorithm: Experience Gathered from Field Experiments

Bernard H. Fleury[(1)], **Xuefeng Yin**[(1)], **Klaus G. Rohbrandt**[(1)], **Patrik Jourdan**[(2)], **Andreas Stucki**[(2)]

[(1)] ***Center for PersonKommunikation, Aalborg University, DK-9220 Aalborg, Denmark, bfl@kom.auc.dk***

[(2)] ***Elektrobit AG, Rosswiesstrasse 29, CH-8608 Bubikon, Switzerland***

Abstract

This contribution reports and discusses results from an experimental investigation of dispersion in delay, direction of departure, and direction of incidence at 2.45 GHz in a typical NLOS pico-cellular environment using the ISI-SAGE (Improved Search and Initialization Space-Alternating Generalized Expectation-Maximization) algorithm presented in [1] and [2]. Most of the estimated waves can be related to the environment under the assumption of one- and two-bounce scattering. The results demonstrate the high potential of the technique for getting a detailed insight into the mechanisms by which the electromagnetic energy propagates between the transmitter and receiver sites. This detailed knowledge is of paramount importance for the development of realistic and accurate models of the radio channel – either for field prediction or for system design – and for MIMO applications.

1 Introduction

It has been recently recognized that the deployment of multiple element arrays at both transmitter (Tx) and receiver (Rx) combined with appropriate coding can substantially increase the capacity of mobile radio communication systems [3], [4], and [5]. The development, i.e. design and performance analysis of such systems employing these so-called smart antennae requires realistic models of the radio channel that incorporate dispersion in direction jointly at the Tx and Rx locations. Experimental validation is a prerequisite to ensure that these models capture the critical features of the physical radio channel. Here, the attribute "critical" designates features potentially affecting the performance of the communication systems under consideration. This validation procedure relies on comprehensive experimental investigations of the radio channel, which demand sophisticated, computationally efficient estimation tools.

In [1] and [2] a high-resolution scheme based on the SAGE algorithm is proposed that jointly estimates the complex weight, the relative delay, the Doppler frequency, the direction, i.e. azimuth and coelevation angles, of departure, and the direction of arrival of waves propagating between the Tx and the Rx. The behaviour of the SAGE algorithm in synthetic channels has been investigated in the former reference as well as in a previous work [6]. In [2] the algorithm is upgraded with an improved search and initialization procedure that speeds up its convergence and enhances the probability of detection for weak paths. This contribution presents experimental investigations where the ISI-SAGE algorithm is applied to measurement data. The reader is referred to [1], [2] and [6] for the description of the underlying signal model and the SAGE algorithm.

Section 2 describes a simple ray-tracing method to reconstruct the propagation path of the estimated waves based on their parameter estimates. The method assumes one- and two-bounce scattering. Section 3 discusses an application of this method to waves estimated in a non-line-of-sight (NLOS) scenario characteristic of pico-cellular environments.

2 Reconstruction of the propagation paths

In this subsection a simple ray-tracing method is proposed that attempts to reconstruct the propagation paths from the wave parameter estimates. The reconstruction procedure assumes that the estimated waves propagate via one- or two-bounce scattering.

2.1 One-bounce scattering

For each estimated wave a region – called scatterer region – is computed that contains a scatterer with which the wave interacts in a one-bounce propagation scenario. Three zones likely to contain the scatterer are calculated while assuming an uncertainty in the estimation of each of the three following parameters: incidence direction, direction of departure, and delay. The scatterer region of a given estimated wave is the intersection of the three uncertainty zones. If this intersection

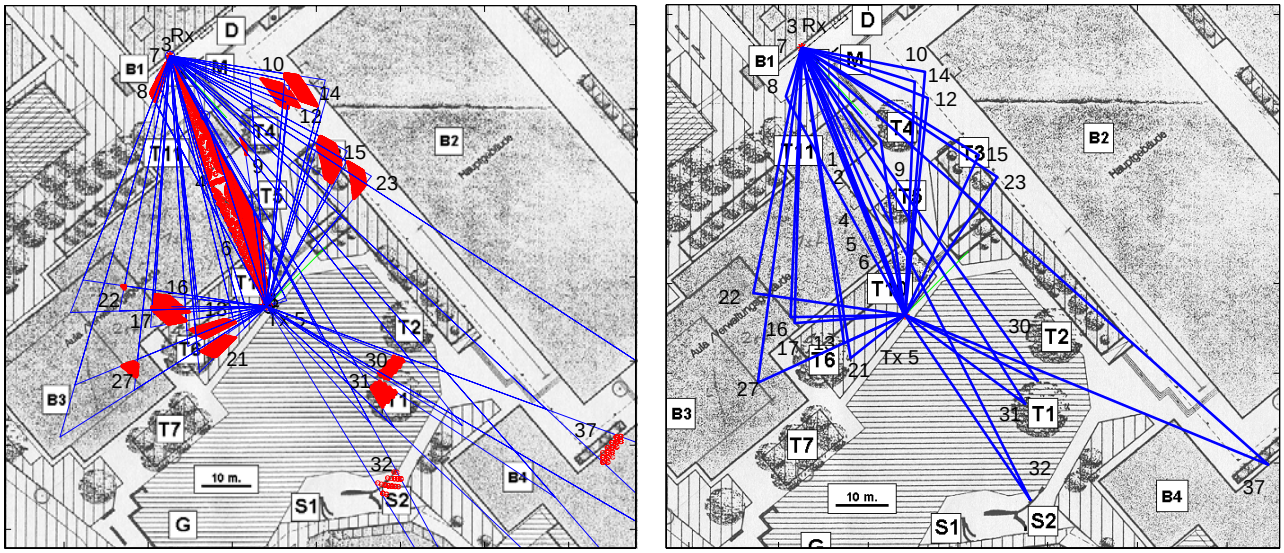

(a) (b)

Figure 1: (a) Reconstructed scatterer regions assuming one-bounce propagation. (b) Reconstructed one-bounce propagation paths. Notice that the reported layout of B2 is the ground floor of this building. The higher floor facade coincides with the dotted line running along this layout.

is non-empty, it is concluded that the wave propagates via one-bounce scattering. Visual inspection of the map should confirm or infirm the presence of at least one significant object in the scatterer region. If such an object exists it is identified to be the scatterer with which the wave interacts.

The uncertainty ranges in delay, direction of departure, and direction of incidence arise as a consequence of various sources of inaccuracy in the measurement process and in the used map. Worth mentioning among these sources are the inaccuracy in the determination of the (absolute) reference time, of the Tx and Rx locations, of the orientation of the antenna arrays, the inaccuracy in the positions of the buildings and structures reported on the map, the direction-dependent resolution ability of the arrays, the effect of diffuse scattering [7], and the channel noise. The uncertainty range in delay is set equal to $\pm 0.5 T_{\mathrm{c}} = \pm 5$ ns around the estimated value. The uncertainty in incidence azimuth, azimuth of departure, and incidence coelevation was found to be $\pm 5^{\circ}$. Because of the poor resolution ability in coelevation of the used Tx antenna array, the uncertainty range of this parameter was selected to coincide with its whole range $[0, \pi]$.

2.2 Two-bounce scattering

A two-bounce path is constructed for the estimated waves to which no one-bounce path could be inferred by means of the method described in the previous subsection. For each of these waves two rays are launched from, respectively, the Tx location in the estimated direction of departure and the Rx position in the estimated direction of incidence. Pairs of points – one point along each ray – are then identified which when they are joined lead to a two-bounce path of which the distance is consistent with the estimated propagation delay within an uncertainty of $\pm 0.1 T_{\mathrm{c}} = \pm 1$ ns. The selected two-bounce path has its two edges close to a significant object/structure in the environment.

3 Experimental investigations

The ISI-SAGE algorithm was applied to measurement data collected at a carrier frequency 2.45 GHz. The measurements were performed with the channel sounder PropSound designed by the company Elektrobit AG, Switzerland. The Rx was equipped with a 4×4 uniform planar array of which the plane was oriented vertically. The Tx was equipped with an array consisting of seven half-a-wavelength spaced elements located on a circle and an element in the center of the circle. The plane of the Tx array was horizontal.

The considered propagation scenarios are characteristic of pico–cellular environments. A map of the surroundings is depicted in Fig. 1. The Rx was located on the second floor of Building B1. The plane of the Rx antenna array was approximately parallel to the south facade of Building B1. Fig. 2 provides a view from the Rx towards the Tx location. The buildings labeled with B2 and B3 on the map appear, respectively, left and bottom right on the photograph. The results reported below were obtained from measurements performed in a NLOS scenario where the Tx was positioned behind

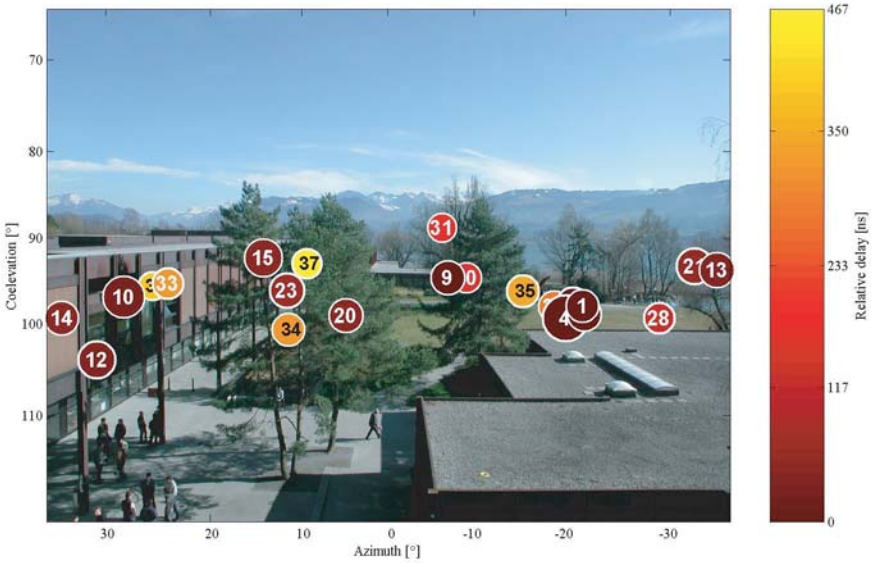

Figure 2: View from the Rx towards the Tx location. The estimated incidence directions falling into the photograph's field of vision are superimposed.

Building B3 (Position Tx 5 on the map in Fig. 1). Other scenarios were also investigated which cannot be discussed here due to the limited amount of space.

The selected set-up of the ISI-SAGE algorithm was as follows: Fifty waves were estimated from ten measurement cycles. The power of the estimated waves ranges from 15.6 dB to 43.9 dB with respect to the noise power. Among the fifty estimated waves those are retained for which the estimated Doppler frequency is confined within ± 0.2 Hz around the frequency offset of the measurement equipment. This selection is reasonable as the environment could be considered as time-invariant during the measurement period. Thirteen waves are removed with this procedure. The remaining thirty-seven waves are ranked in reverse order of their estimated delay, i.e. the wave with the shortest delay has rank 1.

Reported in Figure 2 in form of dots are the estimated incidence directions that fall into the photograph's field of vision. The radius of a dot depends linearly on the magnitude in dB of the estimated complex weight. Wave 4 and Wave 36 have respectively maximum (43.9 dB) and minimum (15.6 dB) absolute complex weight. The dot representing the incidence direction of Wave 36 is behind that of Wave 33 on the photograph. The darkness of a dot codes the estimated delay according to the colour bar reported right to the photograph.

From the thirty-seven estimated waves, twenty-four were categorized as propagating via one-bounce scattering according to the method presented in Subsection 2.1. The derived scatterer regions of these waves are depicted in Fig. 1(a). In each scatterer region a significant object/structure can be identified. Fig. 1(b) illustrates the one-bounce propagation paths passing through these objects/structures. It can be seen that one-bounce propagation occurs via diffraction around roof corner (Waves 1, 2, 4, 5, 6), scattering/reflection on facades (B1: Waves 3, 7; B2: 10, 12, 14, 15, 23; B3: 16, 17, 22, 27; B4: 37), on the metallic sculpture S2 (Wave 32), and diffraction by trees (T1: Waves 30, 31; T6: 13, 21; T4: 9; T11: 8).

A two-bounce path could be inferred for eight among the thirteen remaining estimated waves by using the method described in Subsection 2.2. These paths are reported in Fig. 3. Double-bounce propagation occurs via facade – facade (B4–B2: Waves 33, 34; B3–B1: 18, 19; B2–B1: 11), tree – facade (T6–B2: Waves 25, 26), facade – superstructure (B3–S2: Wave 35). Notice that wave interactions with the south facade of B1 actually occur with various elements of this facade such as metallic window uprights, fore-roof, external items, etc.

Five estimated waves could not be related to the environment under the assumption of one- or two-bounce scattering. Propagation paths with more than two bounces could be identified that are consistent with the estimated parameters of some of these waves. However, more sophisticated validation procedures are required to infer wave interactions with more than two objects/structures.

4 Conclusions

In this contribution we present experimental investigations of dispersion in delay, direction of departure, and direction of incidence in a typical NLOS pico-cellular environment. The wave parameters are estimated with the ISI-SAGE algorithm

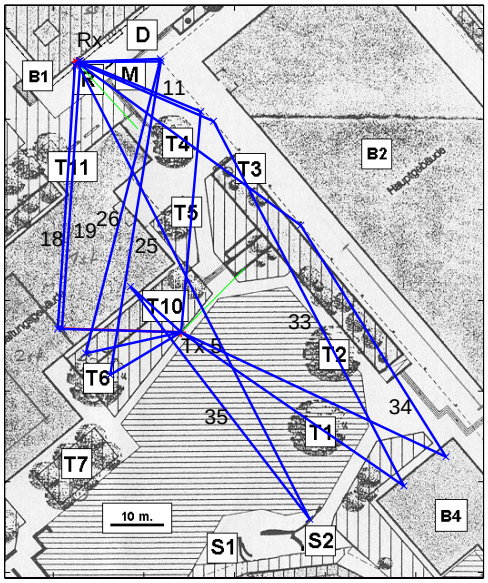

Figure 3: Reconstructed two-bounce propagation paths.

presented in [1] and [2] based on measurement data collected at 2.45 GHz with the channel sounder PropSound.

A simple ray tracing method is proposed to reconstruct the propagation paths of the estimated waves under the assumption of one- and two-bounce scattering. The results show that most estimated waves can be related to the environment by using the above technique. More specifically, significant objects can be identified in the environment which coincide with the interaction points (i.e. the edges) of the propagation paths. Estimated waves can also be identified that are likely to interact more than twice with objects/structures along their propagation path.

The presented investigations demonstrate that resolving waves according to their propagation delay, direction of departure, and incidence direction makes it possible to gain a detailed insight into the main mechanisms by which the electromagnetic energy propagates between the Tx and Rx locations. For instance the results show evidence that the vegetation plays a much more important role than commonly believed.

The impact of this more detailed characterization is manifold: (i) The accuracy of models for field prediction can be increased by incorporating propagation mechanisms that used to be wrongly neglected or even ignored, (ii) Realistic and accurate stochastic models incorporating delay dispersion and dispersion in direction at both Tx and Rx sites can be designed, (iii) Based on these refined models realistic and accurate stochastic MIMO radio channel models can then be derived.

References

[1] B. H. Fleury, P. Jourdan, and A. Stucki, "High-resolution channel parameter estimation for MIMO applications using the SAGE algorithm," in *2002 Int. Zurich Seminar on Broadband Communications (IZS 2002)*, 2002.

[2] B. H. Fleury, X. Yin, K. G. Rohbrandt, P. Jourdan, and A. Stucki, "Performance of a high-resolution scheme for joint estimation of delay and bidirection dispersion in the radio channel," in *Proc. IEEE Vehicular Technology Conference (VTC 2002/spring)*, 2002.

[3] I. E. Telatar, "Capacity of multi-antenna gaussian channels," Tech. Rep. #BL0112170-950615-07TM, AT&T Bell Laboratories, 1996.

[4] G. J. Foschini and M. J. Gans, "On limits of wireless communications in a fading environment when using multiple antennas," *Wireless Personal Communications*, vol. 6, pp. 311–335, 1998.

[5] D. Chizhik, G. J. Foschini, and R. A. Valenzuela, "Capacities of multi-element transmit and receive antennas: Correlations and keyholes," *IEE Electronics Letters*, vol. 36, no. 13, pp. 1099–1100, June 2000.

[6] B. H. Fleury, M. Tschudin, R. Heddergott, D. Dahlhaus, and K. L. Pedersen, "Channel parameter estimation in mobile radio environments using the SAGE algorithm," *IEEE Journal on Selected Areas in Communications*, vol. 17, no. 3, pp. 434–450, Mar. 1999.

[7] M. Bengtsson and B. Völker, "On the estimation of azimuth distributions and azimuth spectra," in *Proc. IEEE 54th Vehicular Technology Conference (VTC 2001/fall)*, 2001, vol. 3, pp. 1612–1625.